Carbon 119 (2017) 365–370

Contents lists available at ScienceDirect

Carbon

journal homepage: www.elsevier.com/locate/carbon

Bonding characteristics and electronic structures of the contact interfaces between group 13 metals and carbon nanotubes

Seunghun Jang [a], Jino Im [a], Min Choi [a], Jeong-O. Lee [b], Ki-jeong Kong [a], Hyunju Chang [a, *]

[a] Center for Molecular Modeling and Simulations, Korea Research Institute of Chemical Technology, Daejeon 34114, Republic of Korea
[b] Advanced Material Division, Korea Research Institute of Chemical Technology, Daejeon 34114, Republic of Korea

ARTICLE INFO

Article history:
Received 21 December 2016
Received in revised form
28 March 2017
Accepted 19 April 2017
Available online 21 April 2017

ABSTRACT

The electronic density of states (DOS) in carbon nanotubes (CNTs) was recently measured using a structure comprising a single CNT-based field effect transistor (FET) device with an indium (In) electrode. Here, we report the bonding characteristics and electronic structure of the contact interface between Group 13 metals (In, Ga, Al) and (8,0) semiconducting CNTs using first-principles density functional theory (DFT) calculations. Our calculation results showed that CNTs in contact with Al, Ga, or In surfaces display lower binding energies to their contact metal surfaces than that of Pd surface while also preserving their original electronic properties. These results originate from the absence of d-orbitals in the Group 13 metals near the Fermi level, the large equilibrium distance, and the deficiencies in electron charge density at the metal surfaces. This study deepens our understanding of the contact properties between Group 13 metals and CNTs.

1. Introduction

Since the discovery of carbon nanotubes (CNTs), single CNT field-effect transistor (FET) have attracted attention for their utility in future nanoscale transistor devices [1–6]. CNT-based FETs may be achieved by improving our understanding of the contact properties between a metal electrode and CNTs, because the electronic and structural properties of single CNTs with a nanoscale size are easily influenced by physical or chemical contact with the metal. Although physisorption of CNTs onto metals is characterized by a small binding energy, large equilibrium distance (≥3 Å), and minute change in interface charge (ionic bonding-like charge distributions), chemisorption is associated with a large binding energy, a small equilibrium distance (≤2.5 Å), and strong hybridization among orbitals (covalent bonding-like charge distributions) [7]. The crucial features that determine the bonding characteristics of a metal/CNT contact interface are the lattice mismatch, work function difference, electronic configuration difference, and so on. Among these, the d-orbital energy range (near the Fermi level) of the metal surface is important because the strength and energy range characterizing the orbital hybridization interactions depend on the degree to which the metal d-orbital energy matches the CNT π-orbital energy. Like this, in various aspects, the continuous studies at atomic level for various metal/carbon-nanomaterial interfaces are mandatory for the achievement and optimization of CNT-based device in an atomic scale. In response to these needs, many fundamental experimental and theoretical studies of metal/CNT contact interfaces have been conducted over the past decade [8–11]. However, there is no systematic studies of the Group 13 metal contacts.

Our group recently reported the possibility of observing the electronic density of states (DOS) of CNTs using a structure comprising a single CNT-based FET device having an indium (In) electrode. The interfacial van der Waals (vdW) gap between the In and CNT was found to play a crucial role in preserving the DOS of the CNTs [12]. These observations suggested the possibility of vdW gap tunneling spectroscopy using single CNT-based FETs. The CNT's electronic DOS identified using vdW gap tunneling spectroscopy in a CNT-based FET device can also suggest a new concept of a memory device in which electrons could be added or extracted from selected energy levels (measured by vdW gap tunneling spectroscopy). Thus, a deeper understanding of the physical phenomena of the In/CNT contact interface is needed. In this work, we considered other Group 13 metals, such as Ga and Al in addition to In metal. The calculated Group 13 metal/CNT contact interface properties were compared with those calculated for a Pd/CNT

* Corresponding author.
E-mail address: hjchang@krict.re.kr (H. Chang).

http://dx.doi.org/10.1016/j.carbon.2017.04.044
0008-6223/

contact structure.

In this study, we examined the bonding characteristics and electronic structures of the contact interface between Group 13 metals (In, Ga, Al) and (8,0) semiconducting CNTs using first principles density functional theory (DFT) calculations. Our calculation results revealed that CNTs on an In, Ga, or Al surface displayed lower binding energies with their contact metal surfaces than that of Pd surface, and they preserved their original electronic properties. These investigations deepen our understanding of the contact properties between Group 13 metals and CNTs, while helping to pave the way for electronic structure measurements in a variety of nanomaterials in weak contact with In or Ga metals.

2. Computational method

The atomic and electronic structures of Group 13 metal/(8,0) CNT and Pd/(8,0) CNT interfaces were examined using the Vienna *ab initio* simulation package (VASP) [13,14]. The exchange-correlation functional was approximated using the Perdew–Burke–Ernzerhof (PBE) expression [15]. The optB86b-vdW functional, implemented in VASP by Klimeš *et al.*, was used in all calculations to account for the weak vdW interactions [16]. Electron–ion interactions were modeled using the projector-augmented wave (PAW) method [17]. The electronic wave functions were expanded in a basis set of plane waves using a kinetic energy cutoff of 500 eV. Geometry relaxation steps were performed under the criterion that the ionic forces were reduced below 0.02 eV/Å. The minimal unit cell of an isolated (8,0) CNT was used as the unit cell along the axial direction (x) of the metal/(8,0) CNT system. To form a two-dimensional metal slab geometry, six or five atomic layers of each metals are excised from the bulk tetragonal (In, space group *I*4/*mmm*, no. 139), orthorhombic (Ga, space group *Cmca*, no. 64), and face centered cubic (Al, Pd, space group *Fm-3m*, no. 225) crystal structures.

Lattice size along axial direction (x) of (8,0) CNT is fixed at the optimized value 2.139 Å, and In, Ga, Al, and Pd metal surfaces' lattice sizes are strained to fit onto CNT's 6 × 1 × 1 (12.835 Å), 2 × 1 × 1 (4.278 Å), 4 × 1 × 1 (8.556 Å), and 4 × 1 × 1 (8.556 Å) super cells, respectively. When adjusting metal's lattice size onto the fixed CNT's lattice, lattice mismatches at all metal/CNT contact structures are smaller than 5% (Table 1). The lattice mismatch between the metal surface and the (8,0) CNTs along the CNT axial direction (x) resulted in compressive strain for In(100), Ga(001), and Al(111) surface, and tensile strain for Pd(111) surface, compared with the experimental values ($A1_{In\text{-}exp}$: 13.000 Å, $A1_{Ga\text{-}exp}$: 4.437 Å, $A1_{Al\text{-}exp}$: 8.591 Å, $A1_{Pd\text{-}exp}$: 8.252 Å, $A1_{exp}$ values are lattice sizes along axial direction (x) estimated from experimental bulk lattice values.) [18,19]. To minimize the interactions between neighboring image cells, vacuum regions at least 16 Å in length along the direction (z) perpendicular to the two-dimensional metal slab were included and the sizes (CNT's central axis to CNT's central axis distances) of all super cells in y-direction were at least ~ 19 Å in all interface models.

3. Results and discussion

Fig. 1 shows cross-sectional side (upper) and top (lower) views of the optimized geometries of the (8,0) CNTs on the (a) In(100), (b) Ga(001), (c) Al(111), and (d) Pd(111) surfaces. Interestingly, circular cross-sectional images of the CNTs in the In/CNT, Ga/CNT, and Al/CNT contacts were indistinguishable from those obtained from the isolated (8,0) CNTs. These contacts were characterized by a relatively large equilibrium distance of 3 Å. By contrast, CNTs in the Pd/CNT contact interface assumed a flat deformation configuration with a large contact area and short equilibrium distance (see Fig. S1). As expected, CNTs in contact with the In, Ga, and Al surfaces deformed to a very small degree (0.007–0.017) (as defined in the Supporting Information) and resembled isolated CNTs, indicating that the intrinsic cylindrical structures of the CNTs in the Group 13 metal/CNT contact interfaces were well-preserved. By contrast, CNTs on a Pd surface deformed to a larger degree (0.117) due to chemisorption between the Pd surface and the CNTs.

The binding energies of all metal/CNT structures were calculated (listed in Table 1) to identify the bonding characteristics of each metal/CNT contact. The binding energy was defined by $E_b = E_{Metal\text{-}surface/CNT} - (E_{Metal\text{-}surface} + E_{CNT})$, where $E_{Metal\text{-}surface/CNT}$, $E_{Metal\text{-}surface}$, and E_{CNT} are the total energies of the metal/CNT contact structures, pure metal surfaces, and the isolated CNT, respectively. The In/CNT, Ga/CNT, and Al/CNT contacts had similar binding energies; however, the Pd/CNT contacts displayed a strong binding energy that was three times the binding energy of In/CNT.

The changes in the electronic properties at the metal/CNT interface were examined by calculating the projected density of states (PDOS) in the (8,0) CNTs in contact with the In(100), Ga(100), Al(111), and Pd(111) surfaces, as shown in Fig. 2(a)–(d). Note that CNTs in contact with the In, Ga, and Al surfaces preserved their original electronic properties, which shifted only slightly toward lower energies. This slight shift was expected because the work functions of In, Ga, and Al are smaller than that of CNT, as shown in Table 1. Because the work function difference between the Ga metal surface and the isolated CNTs was quite small, the DOS shift observed in Fig. 2(b) was also small. By contrast, The semiconducting properties of (8,0) CNT disappeared in the Pd/CNT contact interface due to the Pd metal–carbon electronic interaction.

Additionally, the preservation of the original PDOS of CNTs in contacts with Group 13 metals, which differed significantly from Pd metal contacts was deeply investigated by calculating the PDOS of a pure metal surface, as shown in Fig. 3. The Group 13 metals (Al, Ga, and In) were characterized by a valence electronic configuration of $[X]ns^2np^1$, whereas the Pd metal had a configuration $[Kr]4d^{10}$. The pure Group 13 metal *d*-orbital energies did not overlap with the CNT *p* state energy near the Fermi level (E_F). Note that Al also does not have a *d*-orbital, and the *d* band energies of Ga and In are

Table 1
Energetic and structural properties of the metal/CNT surfaces considered in this work.

	d_{eq} (Å)	E_b (eV/C atom)	WF (eV)	Lattice Mismatch (%)	Tunneling Probability
In(100)/CNT	3.17	−0.026	3.81	−1.3	0.131
Ga(001)/CNT	3.21	−0.024	4.56	−3.6	0.078
Al(111)/CNT	3.15	−0.026	4.18	−0.3	0.129
Pd(111)/CNT	2.04	−0.073	5.41	+ 3.7	1.000

*d_{eq}: The calculated equilibrium separation distances between the lowest carbon atoms of the CNTs and the uppermost metal atoms under the CNTs.
*E_b: The calculated binding energies between the CNTs and the metal surface, per a carbon atom in the metal/CNT contacts.
*WF: The calculated work functions of bare metal surfaces. (The work function of an isolated (8,0) CNT is 4.75 eV).
*Lattice Mismatch: Calculated lattice mismatch between the CNTs and metal surfaces, calculated along the direction (x) parallel to the CNTs.
*Tunneling Probability: The calculated tunneling probability between the CNTs and the metal surfaces along a direction (z) perpendicular to the CNTs.

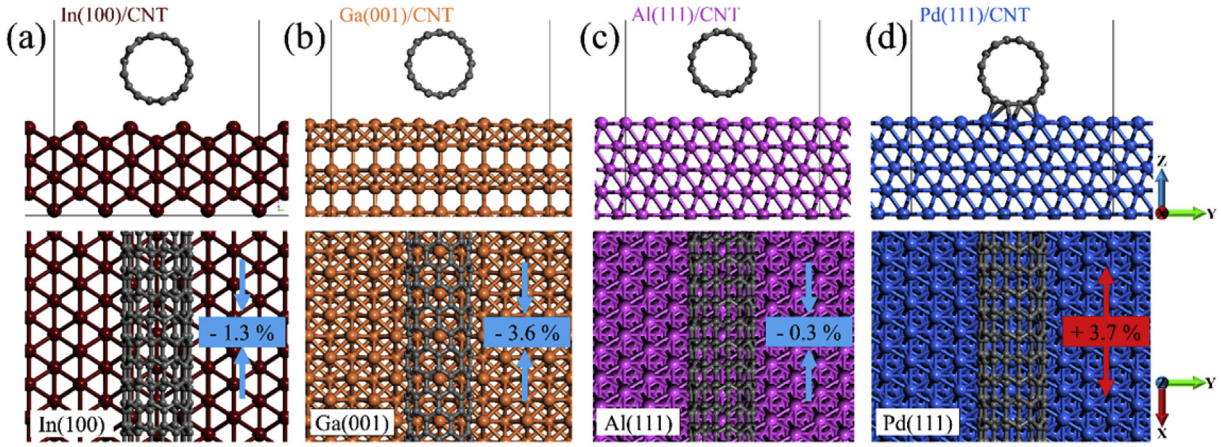

Fig. 1. Cross-sectional side (upper) and top (lower) views of the optimized geometries of (8,0) CNTs in contact with (a) In(100), (b) Ga(001), (c) Al(111), or (d) Pd(111) surfaces. The gray, brown, orange, pink, and blue balls represent C, In, Ga, Al, and Pd atoms, respectively. (A colour version of this figure can be viewed online.)

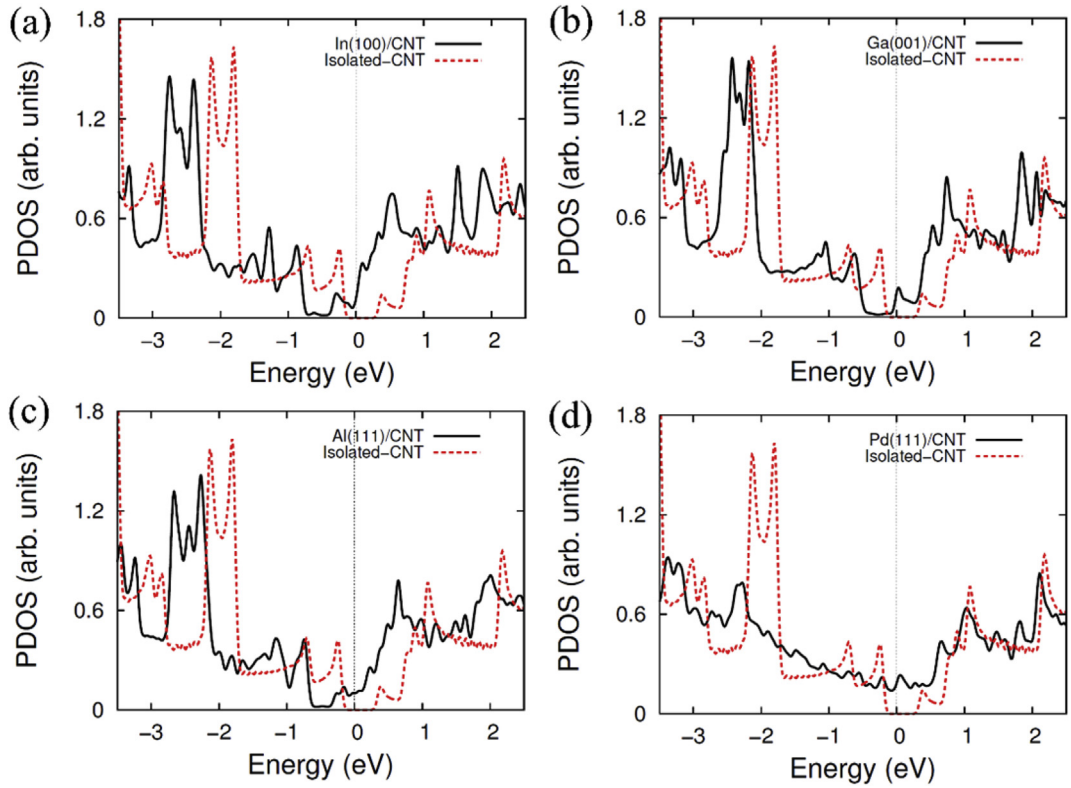

Fig. 2. Calculated PDOSs for (8, 0) CNTs in contacts with the (a) In(100), (b) Ga(001), (c) Al(111), and (d) Pd(111) surfaces. The red dashed lines represent the PDOSs for the isolated (8,0) CNTs. The Fermi levels of all calculated systems were set to zero. (A colour version of this figure can be viewed online.)

about −18.7 (3d) and −16.9 (4d) eV [20]. By contrast, the *d*-orbitals of Pd are located near the E_F level, between −5 and 1 eV; therefore, the PDOS of CNTs on the Pd surface changed entirely, as shown in Fig. 2(d). Gong *et al.* also reported that the strong hybridization interaction involving a metal's *d*-states can modify graphene's π-states [21]. This *p*–*d* orbital hybridization can explain why contact with Pd metal changes a CNT's electronic properties significantly, whereas Group 13 metal contacts preserve a CNT's original electronic properties. It should be noted that Pd metal forms chemical contacts with CNTs, whereas Group 13 metals form physical contacts with CNTs. Meanwhile, in order to check the influence of weak strain on the electronic structure in metal surface, we calculated PDOSs at different strains (tensile and compressive uniaxial strains along the x-direction) for the pure In(100) metal surface, as a representative case. As shown in Fig. S2 (b), *d*-orbital of In metal near the E_F was hardly changed by weak strain and still have low peaks. These results indicate electronic structure of metal is not affected by weak strain at least within applied strain range (see Table 1) of metals used in our calculation.

The chemical contacts made with Pd metal were explored by calculating the PDOSs of fixed CNTs held at various distances from a Pd surface (see Fig. S3). The distance between a CNT and the Pd metal surface most strongly affected the metallic PDOS near the E_F. These results revealed that a distance of about 2 Å provided an

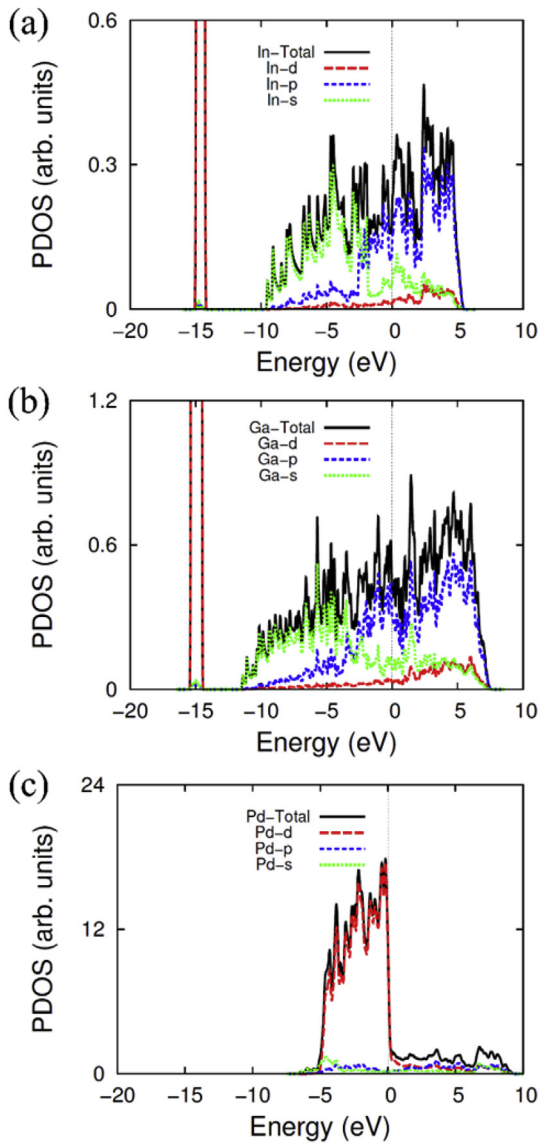

Fig. 3. Calculated PDOSs for the pure (a) In(100), (b) Ga(001), and (c) Pd(111) metal surfaces. The Fermi levels of the three metal surface systems were set to zero. (A colour version of this figure can be viewed online.)

environment in which chemical bonding was possible. As mentioned above, CNT's PDOS in In/CNT, Ga/CNT, and Al/CNT contacts are preserved because the distances between the metal surfaces and the CNTs exceed 3 Å.

As shown in Fig. 4, the energy band structure of a Ga/CNT contact was calculated as a representative case in which the intrinsic electronic DOS of a CNT was preserved. The energy dispersion (black dots) observed in a CNT on a Ga (100) surface was similar to the energy dispersion (red dashed line) observed in an isolated (8,0) CNT. The energy band dispersion of a CNT in an In(110)/CNT contact retained its original electronic properties, as demonstrated previously [12].

Fig. 5 shows charge density difference plots and XY-averaged charge density differences of the In(100)/CNT, Ga(001)/CNT, Al(111)/CNT, and Pd(111)/CNT contacts. Fig. 5(e)–(h) shows the charge density difference, $\Delta\rho = \rho[\text{metal/CNT}] - \{\rho[\text{CNT}] + \rho[\text{metal}]\}$, averaged over the translucent blue box shown in Fig. 5(a)–(d). ρ[metal/CNT], ρ[metal], and ρ[CNT] are the charge densities of the metal/CNT contact structures, pure metal surfaces, and the isolated CNT, respectively. The charge difference plots results presented in Fig. 5 indicated that the In/CNT, Ga/CNT, and Al/CNT contacts underwent minimal electron redistribution. Why might electron transfer be minimal in these three metal/CNT contacts? To answer this question, we calculated the changes in the XY-averaged charge densities near the topmost layer in the corresponding bare metal surfaces, as shown in Fig. S4. The charge density varied from 0.7 Å to 1.3 Å in the topmost layer of the metal surface and reached its largest value in the case of the Pd(111) surface. These results suggested that the electron density near the metal surface affected electron transfer between the metal and CNT.

On the other hand, electron mixing in the Pd/CNT contact interface due to interactions between the *d* orbitals of the Pd surface and the *p* orbital in the CNTs was strong, whereas CNT contact interfaces involving In or Ga metal surfaces displayed weak orbital hybridization between the metal *d* and CNT *p* orbitals. The shape of the isosurface, shown in Fig. 5(a), suggests that the weak interaction resulted from ionic bonding between the π orbitals of the CNT and the p_z orbitals of the In metal surfaces.

Fig. 6 presents the XY-averaged electrostatic potentials obtained from the (a) In(100)/CNT, (b) Ga(001)/CNT, (c) Al(111)/CNT, and (d) Pd(111)/CNT contacts, plotted along the direction (z) perpendicular to the metal surfaces, as shown in the insets of Fig. 6. The barrier heights were 2.79, 3.56, and 3.00 eV in Fig. 6(a)–(c), respectively.

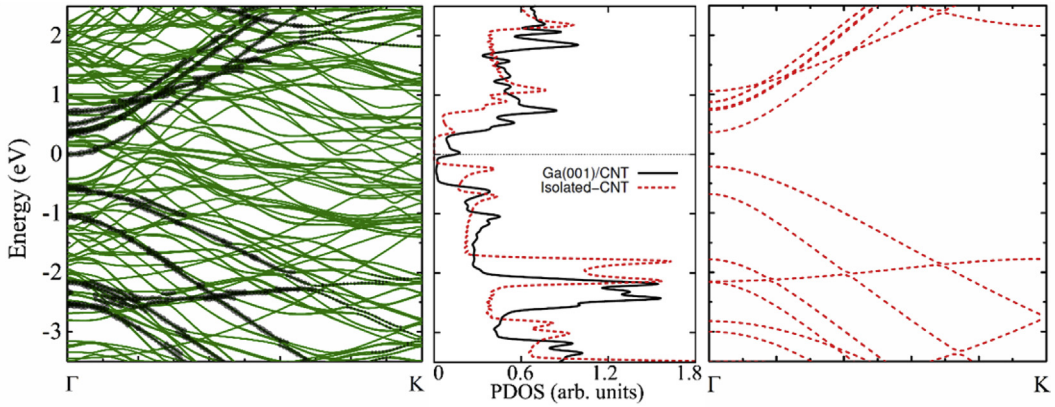

Fig. 4. Calculated band structures (left, black dots) and PDOSs (center, solid black lines) for an (8, 0) CNT in contact with a Ga(001) surface. The relative amount of C $2p_z$ is proportional to the size of the black dots. Solid green lines represent the band structures for Ga(001) surface. The Fermi levels of all calculated systems were set to zero, and the red dashed lines represent the PDOS (center) and band structure (right) of the isolated CNT system. (A colour version of this figure can be viewed online.)

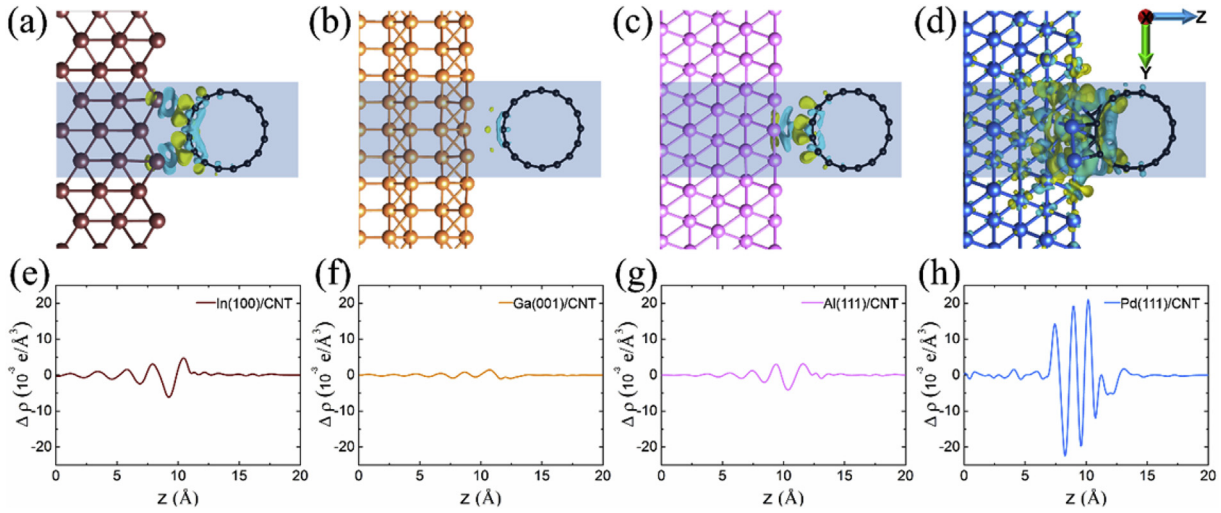

Fig. 5. Charge density difference plots for the (a) In(100)/CNT, (b) Ga(001)/CNT, (c) Al(111)/CNT, and (d) Pd(111)/CNT contacts. The black, brown, orange, pink, and blue balls represent C, In, Ga, Al, and Pd atoms, respectively. The yellow and blue iso-surfaces ($\pm 2.7 \times 10^{-3}$ e/Å^3) corresponded to the electron charge accumulation and depletion zones, respectively. (e) The XY-averaged charge density differences observed in the (e) In(100)/CNT, (f) Ga(001)/CNT, (g) Al(111)/CNT, and (h) Pd(111)/CNT contacts, plotted along a direction (z) perpendicular to the metal surface. The charge density differences measured for all metal/CNT contacts were averaged over the translucent blue box, as shown in (a)–(d). (A colour version of this figure can be viewed online.)

The possibility of utilization as a metal electrode of vdW gap tunneling spectroscopy was assessed by calculating the transmission probability using the Wentzel–Kramers–Brillouin (WKB) approximation. For a detailed explanation on how this transmission probability calculates, refer to the Supporting Information of ref. [12]. Numerical calculations predicted transmission probabilities of 0.131, 0.078, 0.129, and 1.00 for In/CNT, Ga/CNT, Al/CNT, and Pd/CNT, respectively. These small transmission probabilities are consistent with the vdW gap between the Group 13 metals and the CNT contacts. Despite similar properties among the Group 13 metals, vdW gap tunneling spectroscopy has only been reported in In/CNT structures because Ga metal has a very low melting point (29.76 °C), presenting significant challenges to the fabrication of stable FET devices. Our calculated results suggested that similar

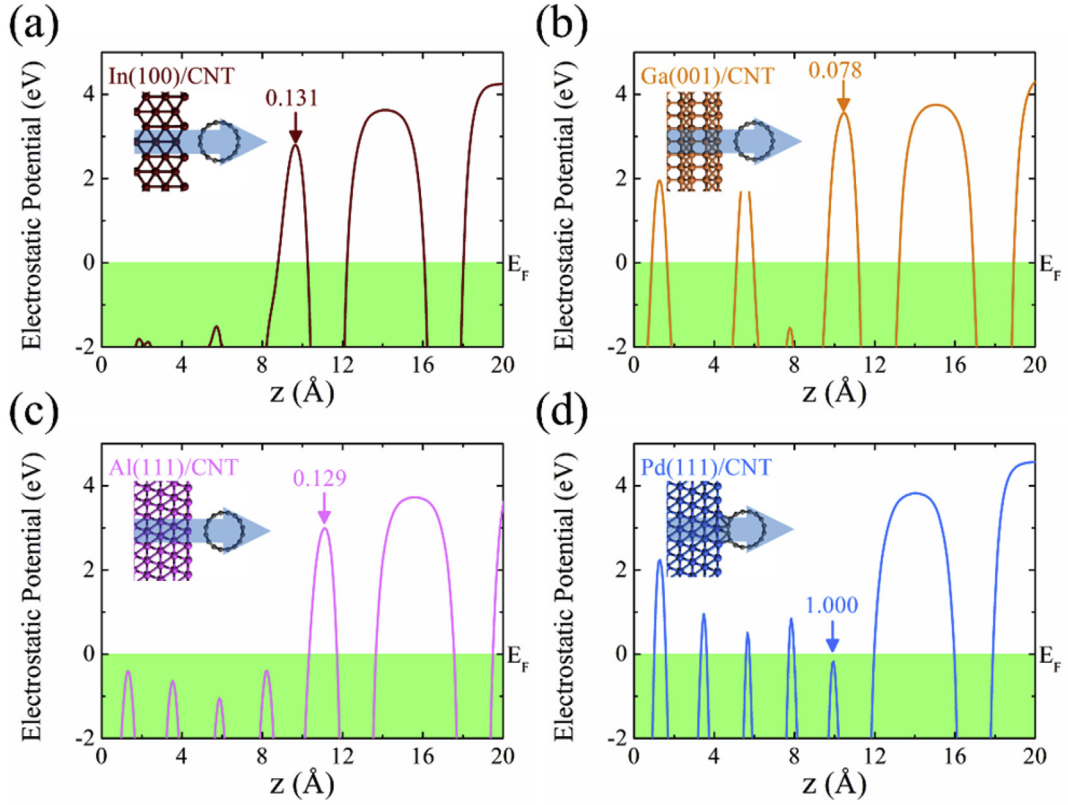

Fig. 6. XY-averaged electrostatic potentials for the (a) In(100)/CNT, (b) Ga(001)/CNT, (c) Al(111)/CNT, and (d) Pd(111)/CNT contacts, which are plotted along a direction (z) perpendicular to the metal surfaces with respect to the Fermi level (E_F). The potentials of the metal/CNT contacts were averaged along the arrows shown in the insets. The electrostatic potential barriers and transmission probabilities at the interfaces of all metal/CNT contacts are indicated by vertical arrows and labels. The transmission probabilities of all contacts were calculated using the Wentzel–Kramers–Brillouin (WKB) approximation. (A colour version of this figure can be viewed online.)

vdW gap properties could be expected in the Al/CNT contact interface as well; however, no such a report of Al/CNT contacts is available, despite numerous experimental studies of Al/CNT contacts. It is interesting to ask why properties similar to those of the In/CNT contact are not observed in the Al/CNT contact. It turns out that the Al surface is more readily oxidized than other Group 13 metal surfaces, as discussed in previous reports [22,23]. Furthermore, the surface oxidation probability may be enhanced at the Al surface due to the large equilibrium distance (3.15 Å) between the Al surface and the CNTs. These properties can explain why only In/CNT contacts display vdW gap tunneling spectroscopy.

So far, we have mainly discussed about the contacts between (8,0) semiconducting CNTs (diameter: ~6.4 Å) and Group 13 metal surfaces. Additionally, we checked the optimized geometry, electronic DOS, and charge density difference of the contact interface between In(100) metal surface and (5,5) metallic CNT with different diameter (~6.85 Å). As shown in Fig. S5 (a) and (b), additional calculation results showed that (5,5) CNT on In surface represented lower BE (- 0.040 eV/C atom) and larger equilibrium distance (3.14 Å) with its contact metal surface than those of Pd surface, and they well preserved their original electronic property. And also, we could see that the contact interface of In(100)/(5,5) CNT showed minimal electron rearrangement (see Fig. S5 (c)). These overall results of In(100)/(5,5) CNT contact are considerably similar to those of In(100)/(8,0) CNT.

4. Conclusion

In conclusion, we investigated the bonding characteristics and electronic structures of the contact interfaces between Group 13 metals (In, Ga, Al) and (8,0) semiconducting CNTs using first principles DFT calculations. The bonding characteristics between Group 13 metals and CNTs were assessed by calculating the optimized structures, binding energies, charge density differences, and transmission probabilities of metal/CNT complex systems. The electronic structures, including the PDOS and band structure, were also calculated. The results obtained from the Group 13 metals/CNT contact interfaces were qualitatively compared with those obtained from a Pd/CNT contact structure, which was simulated as a counterstructure.

The calculations reported here indicated that CNTs adsorbed onto In, Ga, and Al displayed lower energies of binding to their contact metal surfaces than that of Pd surface and preserved the original CNT electronic properties. We found that the contact interfaces showed minimal electron rearrangement, as indicated by the charge density difference calculations of the Group 13 metal/CNT contacts. These results arose from the following effects: (i) *d*-orbitals on pure Group 13 metals near E_F were absent, (ii) the equilibrium distance between the Group 13 metals and CNTs was large, exceeding 3 Å, (iii) and the electron charge density around the Group 13 metal surfaces was deficient.

Lastly, the possibility of utilization as the metal electrodes in vdW gap tunneling spectroscopy was explored by calculating the XY-averaged electrostatic potential and the transmission probability using the WKB approximation. This study deepens our understanding of the contact interface between Group 13 metals and CNTs, while enabling the observation of electronic structures in various nanomaterials in weak bonded contact with In or Ga metals.

Acknowledgment

This research was supported by Nano·Material Technology Development Program through the National Research Foundation of Korea funded by the Ministry of Science, ICT and Future Planning (NRF-2016M3A7B4025408).

Appendix A. Supplementary data

Supplementary data related to this article can be found at http://dx.doi.org/10.1016/j.carbon.2017.04.044.

References

[1] J.W.G. Wilder, L.C. Venema, A.G. Rinzler, R.E. Smalley, C. Dekker, Electronic structure of atomically resolved carbon nanotubes, Nature 391 (1998) 59–62, http://dx.doi.org/10.1038/34139.
[2] R. Martel, T. Schmidt, H.R. Shea, T. Hertel, P. Avouris, Single- and multi-wall carbon nanotube field-effect transistors, Appl. Phys. Lett. 73 (1998) 2447–2449, http://dx.doi.org/10.1063/1.122477.
[3] S.J. Tans, A.R.M. Verschueren, C. Dekker, Room-temperature transistor based on a single carbon nanotube, Nature 393 (1998) 49–52, http://dx.doi.org/10.1038/29954.
[4] J. Charlier, X. Blase, S. Roche, Electronic and transport properties of nanotubes, Rev. Mod. Phys. 79 (2007) 677–732, http://dx.doi.org/10.1103/RevModPhys.79.677.
[5] T. Dürkop, S.A. Getty, E. Cobas, M.S. Fuhrer, Extraordinary mobility in semiconducting carbon nanotubes, Nano Lett. 4 (2004) 35–39, http://dx.doi.org/10.1021/nl034841q.
[6] A.D. Franklin, Z. Chen, Length scaling of carbon nanotube transistors, Nat. Nanotechnol. 5 (2010) 858–862, http://dx.doi.org/10.1038/nnano.2010.220.
[7] Kevin T. Chan, J.B. Neaton, Marvin L. Cohen, First-principles study of metal adatom adsorption on graphene, Phys. Rev. B 77 (2008) 235430, http://dx.doi.org/10.1103/PhysRevB.77.235430.
[8] J. Svensson, E.E.B. Campbell, Schottky barriers in carbon nanotube-metal contacts, J. Appl. Phys. 110 (2011) 111101, http://dx.doi.org/10.1063/1.3664139.
[9] J.A. Rodríguez-Manzo, A. Tolvanen, A.V. Krasheninnikov, K. Nordlund, A. Demortière, F. Banhart, Defect-induced junctions between single- or double-wall carbon nanotubes and metal crystals, Nanoscale 2 (2010) 901–905, http://dx.doi.org/10.1039/C0NR00098A.
[10] A. Fediai, D.A. Ryndyk, G. Seifert, S. Mothes, M. Claus, M. Schröter, G. Cuniberti, Towards an optimal contact metal for CNTFETs, Nanoscale 8 (2016) 10240–10251, http://dx.doi.org/10.1039/C6NR01012A.
[11] B. Ma, C. Gong, Y. Wen, R. Chen, K. Cho, B. Shan, Modulation of contact resistance between metal and graphene by controlling the graphene edge, contact area, and point defects: an ab initio study, J. Appl. Phys. 115 (2014) 183708, http://dx.doi.org/10.1063/1.4876738.
[12] D. Choi, S. Jang, D. Jeong, J. Lee, H. Chang, D. Ha, S.M. Lee, J. Kim, Y.D. Suh, M. Bae, J. Kim, Van-der-Waals-gap tunneling spectroscopy for single-wall carbon nanotubes, Carbon 113 (2017) 237–242, http://dx.doi.org/10.1016/j.carbon.2016.11.053.
[13] G. Kresse, J. Hafner, Ab initio molecular dynamics for liquid metals, Phys. Rev. B 47 (1993) 558, http://dx.doi.org/10.1103/PhysRevB.47.558.
[14] G. Kresse, J. Furthmüller, Efficient iterative schemes for ab initio total-energy calculations using a plane-wave basis set, Phys. Rev. B 54 (1996) 11169, http://dx.doi.org/10.1103/PhysRevB.54.11169.
[15] J.P. Perdew, K. Burke, M. Ernzerhof, Generalized gradient approximation made simple, Phys. Rev. Lett. 77 (1996) 3865–3868, http://dx.doi.org/10.1103/PhysRevLett.77.3865.
[16] J. Klimeš, D.R. Bowler, A. Michaelides, Chemical accuracy for the van der Waals density functional, J. Phys. Condens. Matter 22 (2010) 022201, http://dx.doi.org/10.1088/0953-8984/22/2/022201.
[17] P.E. Blöchl, Projector augmented-wave method, Phys. Rev. B 50 (1994) 17953, http://dx.doi.org/10.1103/PhysRevB.50.17953.
[18] C. Kittel, Introduction to Solid State Physics, seventh ed., Wiley, New York, 1996.
[19] F. I. Z. Karlsruhe, Inorganic Crystal Structure Database, Available at http://icsd.fizkarlsruhe.de.
[20] J.C. Fuggle, N. Mårtensson, Core-level binding energies in metals, J. Electron Spectrosc. Relat. Phenom. 21 (1980) 275, http://dx.doi.org/10.1016/0368-2048(80)85056-0.
[21] C. Gong, G. Lee, B. Shan, E.M. Vogel, R.M. Wallace, K. Cho, First-principles study of metal–graphene interfaces, J. Appl. Phys. 108 (2010) 123711, http://dx.doi.org/10.1063/1.3524232.
[22] N. Park, S. Hong, Electronic structure calculations of metal-nanotube contacts with or without oxygen adsorption, Phys. Rev. B 72 (2005) 045408, http://dx.doi.org/10.1103/PhysRevB.72.045408.
[23] T. Sasaki, T. Ohno, Calculations of the potential-energy surface for dissociation process of O_2 on the Al(111) surface, Phys. Rev. B 60 (1999) 7824–7827, http://dx.doi.org/10.1103/PhysRevB.60.7824.